Wireless Monitoring of Scour and Re-deposited Sediment Evolution at Bridge Foundations based on Soil Electromagnetic Properties

Panagiotis Michalis[1], Alessandro Tarantino[2],
Christos Tachtatzis[3], Martin David Judd[4]

Abstract:

Hydraulic structures constitute the most vulnerable elements of transportation infrastructure. Recent increases in precipitation have resulted in severe and more frequent flash flooding incidents. This has put bridges over waterways at higher risk of failure due to scour. This study presents a new sensor for measuring scour depth variation and sediment deposition processes in the vicinity of the foundations to underpin systems for early warning of impending structural failure. The monitoring system consists of a probe with integrated electromagnetic sensors designed to detect changes in the dielectric permittivity of the surrounding bridge foundation. The probe is equipped with a wireless interface and was evaluated to assess its ability to detect scour and sediment deposition in various soil types and under temperature and water salinity conditions that would commonly occur in a practical installation environment. A novel methodology is also developed enabling discrimination between in-situ and re-deposited sediment delivering vital information about the load bearing capacity of the foundation. The experimental approach was validated using 'static' scour simulations and real-time open channel flume experiments. Results indicate that the sensor is highly sensitive to underwater bed level variations and can provide an economical and accurate structural health monitoring alternative to existing instruments.

Keywords: Structural health monitoring; Geophysics; Electromagnetism; Wireless sensor; Scour; Sediment re-deposition; Soil density; Flood; Bridge foundation.

[1]**Research Associate**, Department of Civil and Environmental Engineering, University of Strathclyde, Glasgow, UK. Email: p.michalis@strath.ac.uk

[2]**Professor**, Department of Civil and Environmental Engineering, University of Strathclyde, Glasgow, UK

[3]**Research Associate**, Department of Electronic and Electrical Engineering, University of Strathclyde, Glasgow, UK

[4]**Technical Director**, High Frequency Diagnostics and Engineering Ltd, Glasgow, UK

1. Introduction

In recent years, severe and more frequent flood incidents across the globe have put bridges at high risk of failure due to scour. Scour is the result of the erosion of streambed around the foundation of a structure, leading to structural instability and ultimately catastrophic failures.

Flood induced scour is the leading cause of bridge failures [1], resulting in loss of lives, traffic disruption and significant economic losses. Scour is expected to occur at most hydraulic structures during their service life [2]. In the UK for example, there are more than 9,000 major bridges over waterways and almost 95,000 bridge spans and culverts susceptible to scour processes. Up to 2003, abutment and pier scour had been identified as the most common cause of more than 130 railway bridge failures associated with fatalities [3]. The damage due to scour action at railway structures alone in the UK is estimated to be over £1 million per year on average [4]. Future projections also indicate that the frequency of extreme flooding across Europe is anticipated to double by 2050 [5] with major implications for highway and railway infrastructure.

Failure of bridges due to scour is attributed to several issues associated with the present visual inspection procedure which often relies on specialist divers. This method is very expensive and time consuming, therefore hydraulic structures are inspected at intervals of several years. Severe scour usually occurs during a flood peak discharge with a high velocity, preventing concurrent diving inspections from being carried out because of safety considerations.

The detection of scoured holes ‘hidden’ by re-deposited soil is also of great importance for the assessment of stability conditions of the foundation. The current post-event visual inspection does not reveal the actual bed level conditions at foundations as re-deposited soil often re-fills the scoured holes. The backfilling material does not have the same resistance to hydrodynamic forces as the in-situ sediment [6] and it is easily scoured again during small-scale floods compromising the integrity of the foundation structure. The majority of the existing monitoring techniques cannot detect sediments re-deposited in scour holes. Furthermore, the ‘as built’ information for many scour critical structures is not available and as a result they are classified as having unknown foundation status [7], making scour risk assessment a particularly challenging issue.

The difficulty of scour monitoring in the field is considered a major gap in the knowledge and general understanding of scour mechanism. Continuous scour monitoring would enable early remedial maintenance and repair actions to be carried out improving public safety and

reducing costs for bridge owners, insurers and maintainers. Real-time data of erosion and sediment deposition processes will also enable the validation of models derived from laboratory-based studies and the assessment of different engineering designs.

2. Current Scour Inspection Techniques

Over recent decades, many techniques have been developed to measure scour action at hydraulic structures. Early research efforts focused on the use of geophysical methods such as seismic-reflection profiling systems and Ground Penetration Radar (GPR) to detect scour at bridge piers and abutments [8, 9, 10]. The same basic principle of wave propagation and reflection is used in both techniques. The seismic profiling systems transmit pulsed acoustic signals at low frequency (in the range of kHz) that propagate through the water to the riverbed. The reflected energy is recorded by a receiver transducer and scour is detected based on the magnitude and the arrival time of the reflected signal [9]. The GPR technique transmits electromagnetic pulses into the ground (typically in the MHz frequency range) and scour is identified based on the electrical properties of the materials by measuring the reflected signals [10]. These methods do not provide real-time evaluation of scour as in the majority of the cases they cannot be used during flood events for safety reasons. Debris, sediment transport and salinity in water greatly affect their signal, requiring expensive and time consuming data processing and interpretation. The scour inspection challenge using these instruments is even greater when considering the need for highly specialised and heavy equipment demanding skilled personnel [9].

Sonar instruments including fathometers, echo sounders and acoustic depth sounders have also been employed to evaluate underwater bed level conditions around piers and abutments [11, 12]. These techniques use the properties of the transmitted and reflected underwater acoustic waves to detect and locate scour holes. However, issues regarding the transducer frequency and debris impact are the major problems for the use of these devices [12]. High sediment concentrations and air entrainment has often negative effects on their readings [6].

In an attempt to address the shortcomings associated with the instrumentations, several monitoring systems were developed to detect scour with sensors permanently installed around a bridge pier or abutment. For example, Time Domain Reflectometry (TDR) [13, 14] and Fiber-optic Bragg Grating (FBG) sensors [15, 16] were investigated. In TDR technology, an electromagnetic pulse is generated and sent through a transmission line which is installed into

the riverbed. The measure of scour is based on the reflection time required from the pulse to propagate through the line. The major challenges with TDR sensors are related to the high cost, the battery life, the maximum practical probe length, their applicability in conductive mediums and the debris impact [13]. In the FBG method a rod is embedded into the sediment and is instrumented with a number of FBG sensors. Scour activity is identified according to the exhibited strain signal of each sensor when exposed to water flow conditions [15]. Another approach of the same technique uses a single FBG sensor for transduction of the vibration frequency. The scour depth is detected based on the inverse relationship between the fundamental frequency and the cantilevered length of the rod which increases as scour occurs [16]. However, for the use of FBG sensors, installation design and improved fabrication techniques are still required to withstand field conditions [15].

The high cost of existing monitoring techniques is identified as the most common reason for the limited use and application of these devices for scour monitoring at hydraulic structures [6]. Other factors are associated with the complexity of the equipment, the capability of providing repeatable and reliable information, the processing and interpretation of data and the harsh environmental conditions.

The aim of this study is to evaluate the capability of a new, low-cost monitoring technique, based on measurement of soil electromagnetic properties, for the detection of scour and sediment deposition processes. The monitoring system uses scour probes embedded into the sediment next to the foundation structure to detect underwater bed level variation. The real-time remote monitoring is achieved via wireless communication technologies that ease installation and reduces costs. The sensor was tested under different environmental conditions in ‘static’ scour simulations and real-time flume experiments.

3. Monitoring Concept

3.1. Soil dielectric properties

Several methods across a wide range of disciplines have employed the electromagnetic properties of materials to determine the moisture content of products that contain water. The major advantage of the electromagnetic measurements in soil samples originates from the sensitivity of the soil dielectric permittivity to its water content. This is due to the large difference between the permittivity value of water ($\varepsilon_w \approx 80$) when compared to dry solid particles ($\varepsilon_s = 3 \div 5$) and air ($\varepsilon_a \approx 1$). In the following text, the term 'permittivity' will refer to the dimensionless 'relative permittivity' (ε_r) unless otherwise stated.

In general, the permittivity is a frequency and temperature dependent complex variable, which describes the ability of a material to polarise when subjected to an alternating electric field. The complex permittivity is composed of the real part ($\varepsilon_r^{'}$), which is a measure of the polarization property of a material, and the imaginary part ($\varepsilon_r^{''}$), that represents the energy dissipation by polarization and ionic conduction losses. The apparent permittivity (ε_m) of a soil mixture is a function of the permittivity of the air, soil and water components and their volume fractions [17]. A three phase mixing model to describe a wet soil sample was also proposed by Roth et al [18]:

$$\varepsilon_m^{\alpha} = \theta \times \varepsilon_w^{\alpha} + (1-\eta) \times \varepsilon_s^{\alpha} + (\eta - \theta) \times \varepsilon_a^{\alpha} \quad (1)$$

where θ is the volumetric water content, η is the porosity of soil, 1-η and η-θ are the volume fractions that correspond to solid and air phases respectively. Several theoretical and experimental studies have been performed in order to determine the factor α, which describes the orientation of the electric field with respect to the geometry of the medium. The dimensionless factor α can theoretically range from α = +1 for an electric field parallel to soil layers, and α = -1 for an electric field perpendicular to soil layers. Birchak et al [19] found α = 0.50 for an isotropic two-phase medium while Dobson et al [20] using a four phase model estimated α = 0.65 by regression of data obtained from various soil types tested in different frequencies. Roth et al [18] inferred from experiments α = 0.46 by a weighted non-linear regression using a three phase mixing model [see equation (1)] at thirteen soil samples.

For the case of a saturated soil sample ($\eta = \theta$), equation (1) reduces to a two phase mixing model:

$$\varepsilon_m^{\alpha} = \eta \times \varepsilon_w^{\alpha} + (1-\eta) \times \varepsilon_s^{\alpha} \quad (2)$$

and can be used to infer the porosity η from the measurement of the soil permittivity (ε_m), once the parameter α is calibrated and the permittivity of the solids (ε_s) calibrated in dry soil or estimated:

$$\eta = \frac{\varepsilon_m^{\alpha} - \varepsilon_s^{\alpha}}{\varepsilon_w^{\alpha} - \varepsilon_s^{\alpha}} \quad (3)$$

In turn, the porosity can be used to calculate the dry density of a soil sample based on the soil specific gravity (G_s) as follows:

$$\rho_d = (1-\eta) \times G_s \quad (4)$$

When the permittivity becomes equal to the permittivity of water ($\varepsilon_m = \varepsilon_w$) then the porosity is calculated equal to 1 ($\eta = 1$) which corresponds to fully scoured conditions.

3.2. Scour probe operating principle

The large contrast in permittivity associated with water and soil having different densities is used to detect scour and sediment deposition processes around the bridge foundations. Figure 1(a) presents an example of the permittivity values calculated from equation (2) assuming that $\alpha = 0.50$, $\varepsilon_s = 4$, and $\varepsilon_w = 80$. Let us also assume that the porosity of saturated soil forming the river bed varies in the range between 0.40 and 0.50. This results in permittivity values ranging from 23 to 30 [see figure 1(a)]. When the saturated soil is fully substituted by water, the porosity will become equal to 1 and the obtained permittivity will reach the value of 80. When soil is deposited and the scour hole is re-filled, the porosity of the soil will decrease. For example, porosity in the range from 0.5 to 0.6 will result in permittivity in the range 30-38. As depicted in figure 1(a), different permittivity values will correspond to pre-scour and post-scour conditions.

The probe is composed of a dielectric rod with multiple sensors along its length that is inserted into an access tube. Each sensor is formed by two electrodes which transmit an electromagnetic field that penetrates the external surrounding medium [see figure 1(b)]. Since the geometric characteristics of the instrument remain constant the sensor output only depends on the dielectric properties of the sediment. The aforementioned principle is employed to develop a scour monitoring solution with wireless data transmission.

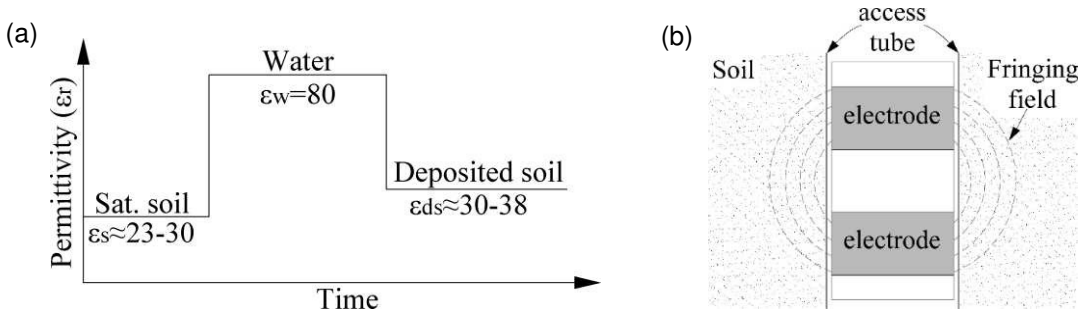

Figure 1: (a) Permittivity values obtained in various porosity conditions and **(b)** electromagnetic fringing field generated between 2 electrodes penetrating the external medium outside the access tube.

A Profile Probe PR2 (Delta-T Devices Ltd) is proposed for scour and sedimentation monitoring interfaced with an off-the shelf wireless device, as shown in figure 2. The probe is composed of a 25 mm diameter hollow shaft equipped with several electromagnetic sensors placed along its length (see figure 2). The complete assembly is then inserted into a fibre glass access tube to protect it from water ingress.

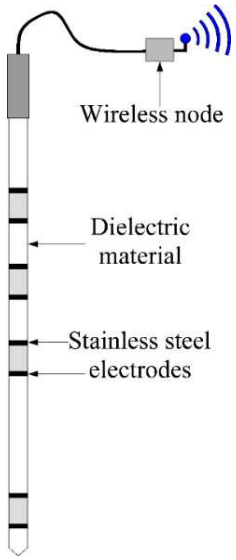

Figure 2: Small-scale off-the-shelf probe equipped with wireless interface.

The two stainless steel rings form the plates of a capacitor in an RLC circuit consisting of Resistive (R), Inductive (L) and Capacitive (C) elements, as shown in figure 3. The PR2 probe measuring principle is based on Amplitude Domain Reflectometry (ADR) method with the complex impedance mainly represented by the sediment or water-filled capacitor [21]. The signal detector is positioned between the signal source and the complex impedance (see figure 3).

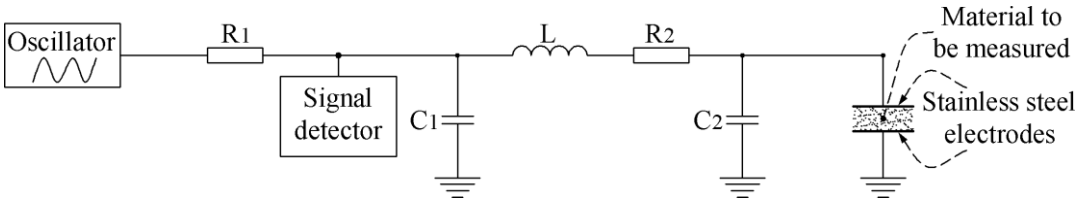

Figure 3: Sensing electronics placed at each sensor location, adapted from [21].

The amplitude output of each sensor is based on the ratio of the incident signal that is generated by the oscillator and the reflected signal that is resulting from the impedance mismatch and is dependant of the medium permittivity. A 6th order polynomial is proposed by the manufacturer to relate the refractive index ($\sqrt{\varepsilon}_r$) of a soil sample to the voltage output of the sensor, as follows [22]:

$$\sqrt{\varepsilon}_r = 1.125 - 5.53 \times V + 67.17 \times V^2 - 234.42 \times V^3 + 413.56 \times V^4 - 356.68 \times V^5 + 121.53 \times V^6 \quad (5)$$

The sensor voltage can therefore be used in order to infer the permittivity of the medium and provide an indication of underwater bed level processes.

The sensor and associated signal detector circuits are located in the shaft and near the sensor location to reduce interference and enhance the signal-to-noise ratio. The sensors are

designed to operate with an input current of 20 mA and at the frequency of 100 MHz, generated by an oscillator. This frequency range is used to reduce the effect of the conductance of the medium and increase sensitivity to soil permittivity [21].

The scour probe was interfaced with a low power AdvanticSys CM 5000 wireless sensor node (82 mm x 33 mm x 7 mm). The CM 5000 is equipped with an IEEE 802.15.4 compatible transceiver (CC2420) with maximum data rate of 250 kbps and a 16-bit MSP430F1611 microcontroller (see figure 4). The microcontroller has an 8-channel and 12-bit Analogue-to-Digital Converter (ADC); the four sensor outputs are each attached to one channel leaving four channels spare for future use or for a longer probe with additional sensors. The device has an on-board antenna that provides a range of 35 m in free space.

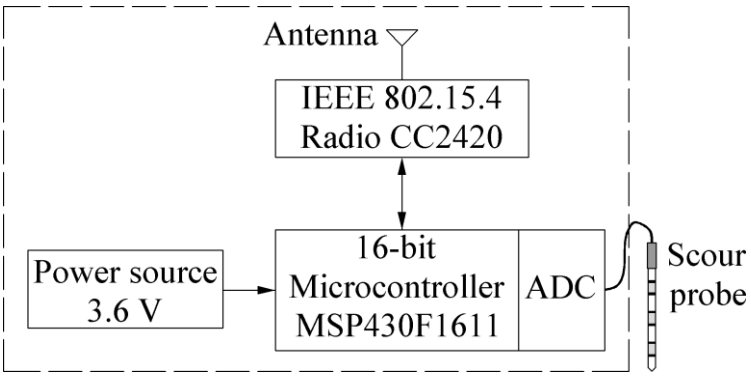

Figure 4: Wireless node components.

The wireless scour probe transmits readings at a configurable interval to an identical device connected to a laptop that acts as a base station. The complete probe assembly and the base station are shown in figure 5.

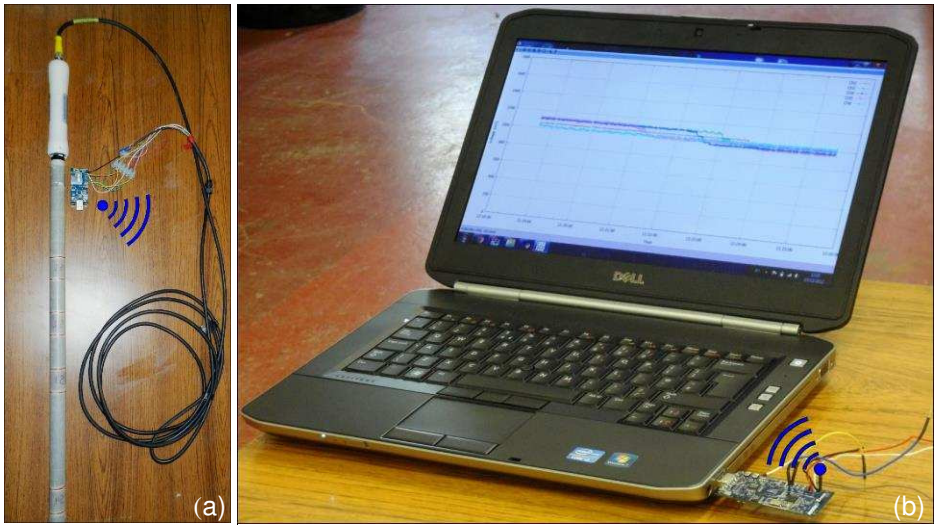

Figure 5: (a) Wireless probe used in the experimental scour tests and **(b)** real-time wireless data transmission to the base station.

3.3. Scour and sediment deposition monitoring implementation

The concept of this scour monitoring solution is illustrated in figure 6 where two probes are installed adjacent to a bridge pier. Each probe can be equipped with several sensors (in this example S1 to S6) placed at predetermined locations. In the example shown in figure 6, sensor S1 is kept in the water above the bed level for reference purposes while the sensors S2 to S6 are embedded into the sediment next to the foundation structure. Figure 6 also shows the typical sensor responses expected when scour and sediment deposition conditions occur.

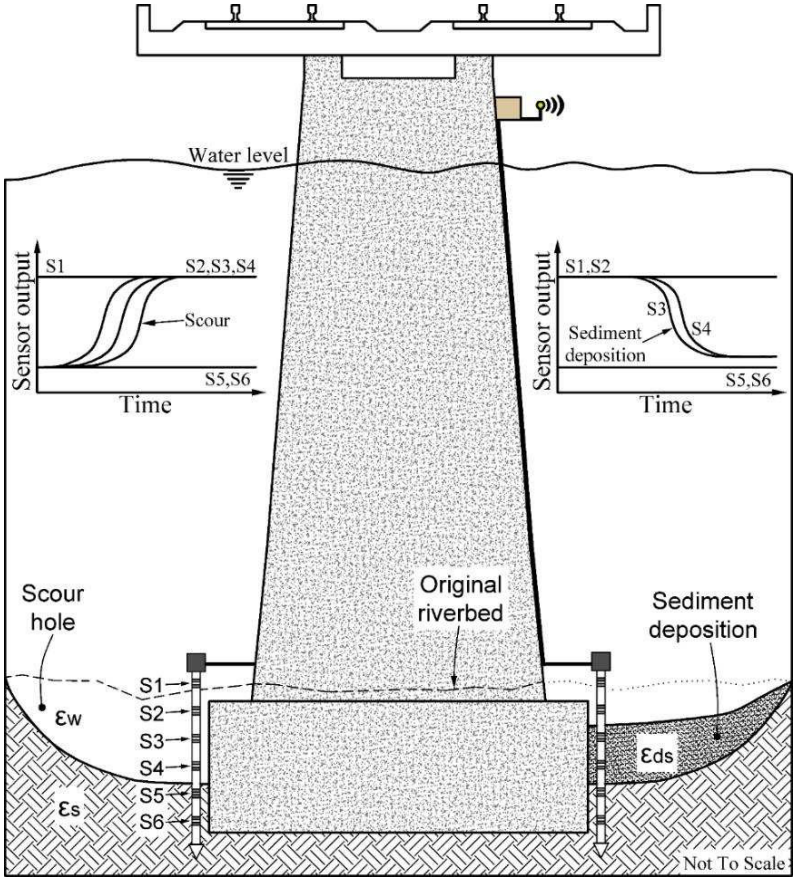

Figure 6: Anticipated amplitude response of the sensors during scour and sedimentation processes.

The sensor submerged in water (S1) is expected to experience higher permittivity and hence show a greater voltage when compared to the sensors that are embedded into the sediment. As scour occurs the composition of the material between the electrode rings is altered due to a change of the permittivity, which impacts the energy stored in the sensor capacitance. As shown in figure 6, the output of the sensors S2, S3 and S4 is increased when the sediment surrounding the sensors is eroded and replaced by water. Sensors S5 and S6 are not affected by scour action and their signals remain constant. The amplitude change is an indication of erosion process around the bridge pier at a depth equal or greater than the location of S4, whose position gives an indication of the minimum scour depth. As depicted in figure 6, during the

sediment deposition process the scour hole is expected to be partially re-filled. Similarly to the conditions that corresponded to scouring, the sensors S1 and S2 which are exposed to water, are anticipated to exhibit higher output due to water permittivity conditions. After deposition, the signals of S3 and S4 are anticipated to settle to values close to S5 and S6. In this scenario, the locations of the sensors S2 and S4 define the minimum range of sediment deposition depth.

4. Experimental Procedures

4.1. Sensor calibration and sensitivity to water salinity and temperature

The response of the ADR probe and the calibration curve scaling the electrical signal to permittivity were initially evaluated by submerging the probe in solvents with known permittivity values. The tests were performed with the probe placed at the centre of a clear acrylic cylindrical tank, with diameter and height of 300 and 600 mm respectively (see figure 7). One sensor was immersed during each experiment and data recorded for the period of ten minutes with an average frequency of four readings per second, using the National Instrument Data Acquisition system (NI cDAQ-9178) interfaced to a computer via LabView programme. The sensor output was recorded in air (ε_r = 1.00) and fresh water (ε_r = 78.54) conditions and then in various solvents with known dielectric constant values [23] that consisted of acetic acid (ε_r = 6.15), acetone (ε_r = 20.70) and methanol (ε_r = 33.62).

Figure 7: Evaluation of the probe in various solvents.

Preliminary experiments revealed temperature and salinity effects on the signals of a sensor that was embedded into various sediment types [24, 25]. Consequently, another set of experiments was carried out to investigate the sensor response in saline water environment at a temperature of 18 ^{o}C. Different salinity solutions were prepared by dissolving in fresh water for each test 0.085 moles (mol) NaCl per litre (L), 0.256 mol NaCl/L, 0.427 mol NaCl/L and 0.598 mol NaCl/L that corresponded to 5 ppt, 15 ppt, 25 ppt and 35 ppt of NaCl respectively.

The temperature influence on the response of the submerged sensor was also evaluated and reported herein using fresh water and saline water of 35 ppt at temperatures of 2 ^{o}C, 11 ^{o}C and 21 ^{o}C.

4.2. Calibration of the soil mixing model

The soil density influence on the probe output is of main importance in this study, as it will be used as a tool to differentiate between the pre-scour (in-situ saturated soil) and post-scour (deposited sediment) conditions. To assess the probe response to density changes one sensor was subjected to a series of experiments in soil samples with various density values. The aforementioned tank was used with the probe placed in the centre and one sensor at a distance of 3 cm from the tank base (see figure 8).

The sample consisted of medium sand with D_{50} of 0.375 mm and specific gravity of 2.83 that was experimentally determined according to the ASTM D 854-00 standard. The medium sand was first dried in a thermostatically controlled oven at the temperature of 110 ^{o}C. The dry sample was weighed and then water was sprayed on the surface of a soil layer and mixed with the sediment in order to attain a target gravimetric moisture content of 10 %. A portion of the sample was also placed in the oven before each experiment in order to determine the actual achieved soil moisture content according to ASTM D2216 standard.

Figure 8: Experimental set up for soil density tests.

The wet sediment was then carefully positioned in layers into the tank and the sensor measurements were recorded. To compact the soil to various target densities, a plywood disk of 290 mm diameter was placed at the top of the sediment to allow distributing the force generated by a hammer dropped on the disk to compact the soil. The hammer consisted of a metal disk attached to Perspex acrylic with weight of 3016 g (see figure 8). Two wooden

handles were fixed in the hammer that was dropped from a distance of 25 cm for 5, 15 and 25 blows in each experiment. The apparent permittivity for the different soil density conditions was measured from the sensor response using equation (5) and was then used to calibrate the parameter α in equation (3).

4.3. 'Static' scour tests

The probe was subjected to a series of 'static' scour simulations in various water conditions using three different soil types. Figure 9(a) shows the experimental setup used to quantify the effect of scour on the probe response. The probe was inserted at the centre of a clear acrylic cylindrical tank with diameter and height of 250 mm and 450 mm respectively [see figure 9(b)]. The real-time response of the sensors was recorded using the AdvanticSys wireless device to transmit measurements to the laptop PC.

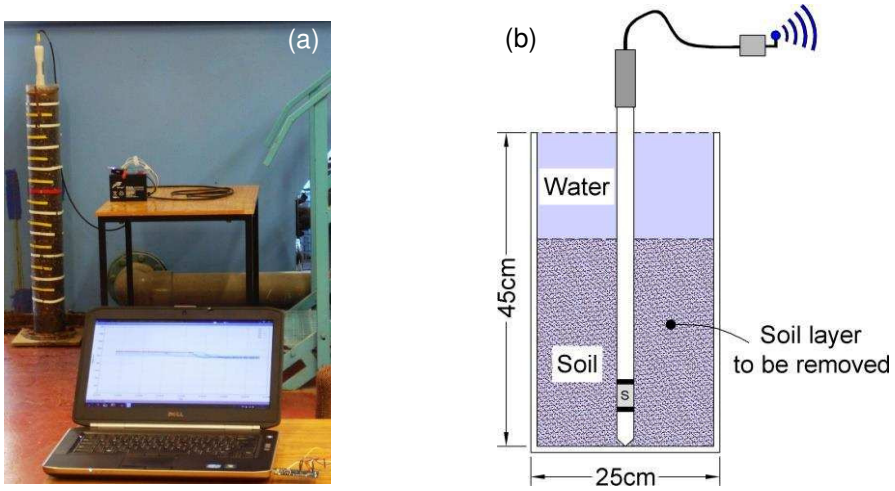

Figure 9: (a) Experimental setup and **(b)** sensor position during 'static' scour tests.

The tested soil types consisted of medium gravel, coarse sand and medium sand with median grain sizes D_{50} of 10 mm, 1.05 mm and 0.375 mm respectively. The probe was placed in the tank which was filled with water and then with un-compacted material. After recording the sensor response, the layer of sediment was removed around the embedded probe in order to mimic the scour process. The tests were performed for each soil type using fresh and saline water of 35 ppt at the temperature of 11 ^{o}C. The purpose of those experiments was to assess the effect of pore water salinity on the sensor output. Based on the soil porosity values estimated from equation (3) in fresh water, the tests in saline water also focused on the comparison between the measured and predicted by equation (2) permittivity values using the parameter α obtained from the previous calibration.

4.4. Flume experimental set up

Real-time scour experiments were conducted in the unidirectional current flume of the hydraulics laboratory located at the University of Strathclyde, Glasgow. The flume (see figure 10) has bottom and sidewalls made of plexiglas supported by a metal frame with a rectangular cross-section of 0.90 m (height) x 0.40 m (width) and 12.0 m (length). A circulation system with a sump and a pump supplies water to the horizontally positioned flume and a valve is used to control the flow discharge and hence, the water depth. The riverbed segment consisted of 0.40 m width and 1.50 m length positioned 6.25 m downstream of the flume entrance and was confined by two smooth plywood plates level with the top surface of the test section. Ramps were used to accommodate the flow to and from the raised bed with slopes of 1/3.75 and 1/2.50 for the upstream and downstream ramps respectively, as shown in figure 10.

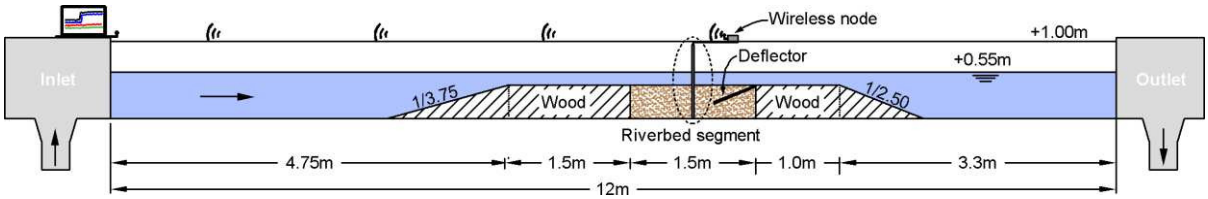

Figure 10: Flume experimental set up.

Preliminary experiments indicated scouring at the interface of the sediment and the plywood downstream plate. A deflector with a slope of 1/2.50 was therefore positioned within the downstream side of the test section to direct the flow away from the interface. Sediment traps were also installed upstream and downstream of the ramps to decrease sediment transportation and re-deposition in the test section while water was re-circulating in the flume.

Separate flume experiments were conducted with two sand soil types; a non-uniform mixture of coarse sand sediments (Coefficient of gradation: C_c = 1.63) with median grain size D_{50} = 0.781 mm and specific gravity of 2.88 and a uniform medium sand (C_c = 1.19) with median grain size D_{50}= 0.375 mm and specific gravity of 2.83. The soil was placed un-compacted to achieve relatively low density values and to accentuate scouring process.

The scour probe was installed in the middle of the riverbed segment and fixed at the bottom of the flume. Although the probe is equipped with six sensors, only four were used in these experiments due to the limited depth of the flume. S1 was placed at 2.0 cm above the surface of the riverbed segment and it remained fully submerged in water during the experiments. S2, S3 and S4 were embedded into the sediment at depths of 2.5 cm, 12.5 cm and 32 cm below the riverbed segment surface as shown in figure 11(a). The wireless interface was

placed 0.5 m downstream of the scour probe and attached to the flume frame while the base station was positioned 7.5 m away, on top of the flume inlet [see figure 11(b)].

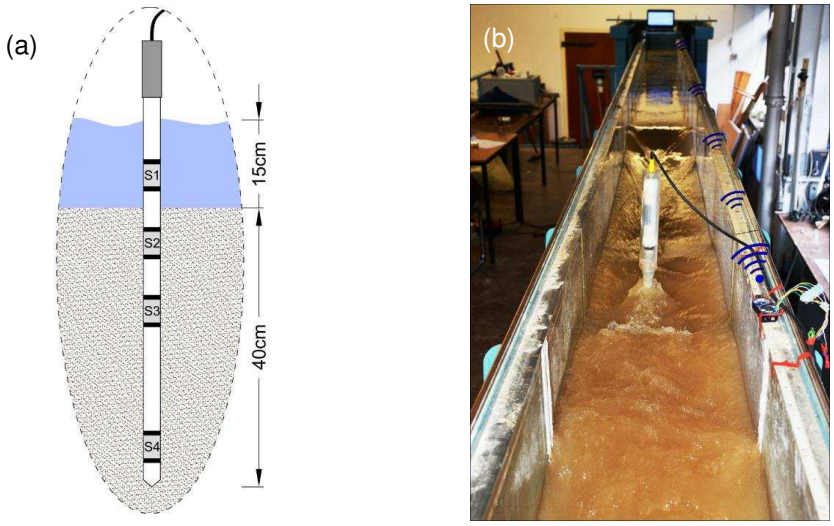

Figure 11: (a) Position of sensors in the riverbed segment; **(b)** wireless node location downstream of the scour probe and data transmission to the base station at the entrance of the flume.

The bed was thoroughly levelled before each experiment and the bed level at the probe position was recorded throughout the experiments with a Vernier point gauge at time intervals of 30 mins. An OTT Hydromet current meter (type: 02 ‘‘10.150’’) connected to NI DAQ (NI USB 6009) interfaced to a computer via LabView recorded the water flow rates in the riverbed segment. A poddymeter instrument located after the valve at the outlet of the downstream tank also provided measurements of the discharge. Prior to initiating flow conditions, the tested section was saturated by allowing water to gently run off the upstream plywood plate for a period of one hour. Experiments started by allowing the water to flow over the horizontal bed with a defined flow rate of 0.40 m/s. During the flume tests the velocity varied in the range from 0.40 m/s to 1.30 m/s and the corresponding water depth at steady state ranged from 0.5 cm to 15 cm respectively. Deposition was simulated by adding 500 g of sediment at intervals of 30 sec on the ramp located on the upstream side of the test section from where the sediment was transported by flow conditions and deposited in the scoured riverbed segment.

Low flow rates generated clear water scour conditions that evolved to live bed and/or general scour in the test section when flow velocity was increased. The duration of each flume experiment was seven hours and the results were collected and analysed.

5. Experimental Results

5.1. Sensor calibration and sensitivity to water salinity and temperature.

The calibration curve provided by the manufacturer relates the sensor output to permittivity [see equation (5)]. This relationship was validated by immersing the sensor in different media with known permittivity in the range of square root between 1 (air) and 8.97 (water) at 20°C. As shown in figure 12, an excellent match was obtained between the predicted and measured values (region i).

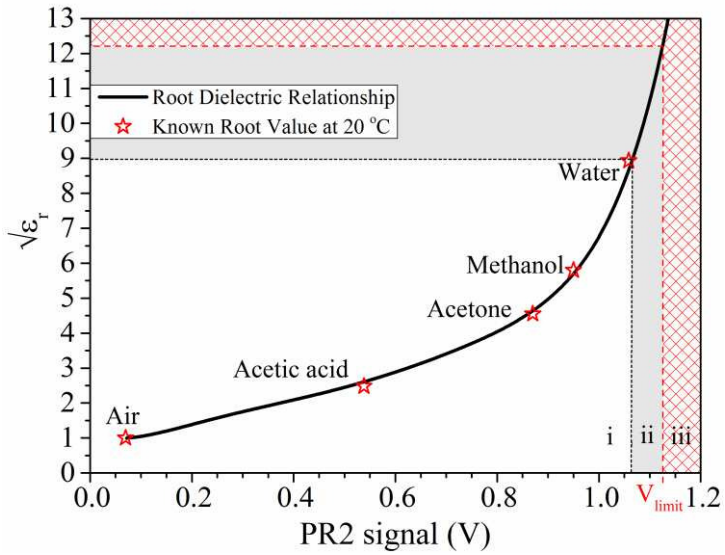

Figure 12: Measured and predicted voltage output in solvents with known dielectric constant values.

Regions (ii) and (iii) in the calibration curve arise from additional experiments that were carried out to evaluate the sensor behaviour in greater permittivity values which are described as follows. In particular, to investigate the effects of salinity on the sensor output, the probe was tested in aqueous solutions with various concentrations at the temperature of 18 °C. Figure 13 presents the response of the sensor in terms of apparent permittivity compared to the values obtained using the equation proposed by Stogryn [26]. At fresh water (0 ppt) and 5 ppt salinity conditions, there is a satisfactory agreement between the predicted and measured values. For concentrations of 15 ppt, 25 ppt and 35 ppt, an almost linear increase of the calculated permittivity is expected using Stogryn's equation, while the measured permittivity remained essentially constant. The sensor output voltage saturates and is unable to detect permittivity values higher than 150 indicating that its dynamic range is limited. This is therefore the reason for the large difference that was obtained between measured and predicted values in the salinity range 15-35 ppt.

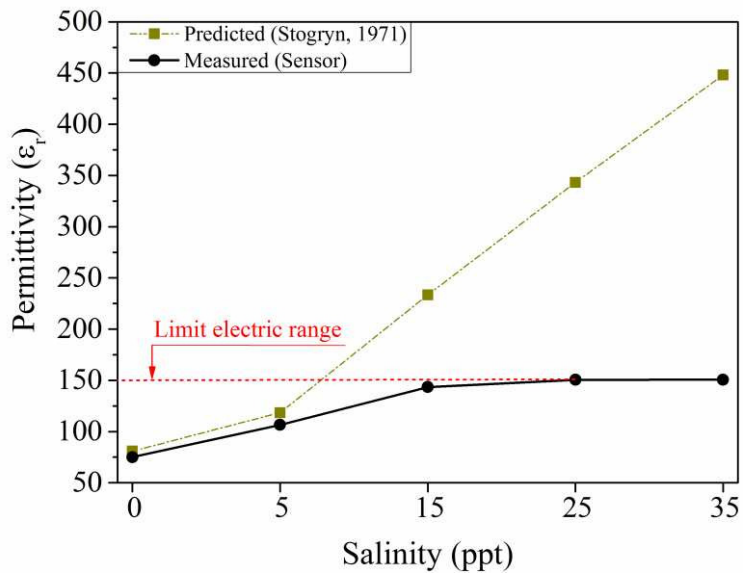

Figure 13: Sensor response in various salinity conditions.

In view of the results in figure 13, two further regions can be identified in the calibration plot shown in figure 12. For square root values between 8.97 and 12.25 (region ii), the instrument is able to measure the permittivity. However, the calibration curve should be considered with care because it has not been validated in this range. Region (iii) exceeds the range of the sensor, as the instrument is not able to output a voltage greater than 1.125 Volts, which corresponds to a root permittivity value of 12.25.

Figure 14(a) shows that permittivity in fresh water decreased with temperature in the range of 2 ºC, 11 ºC and 21 ºC. This trend is in reasonable agreement with the permittivity calculated according to Stogryn [26]. On the other hand, increased temperature in saline water of 35 ppt resulted in a small increase of the sensor output compared to the large increase of values calculated according to Stogryn [26], as shown in figure 14(b). Again, this discrepancy is associated with the attainment of the upper limit of the electrical range of the probe.

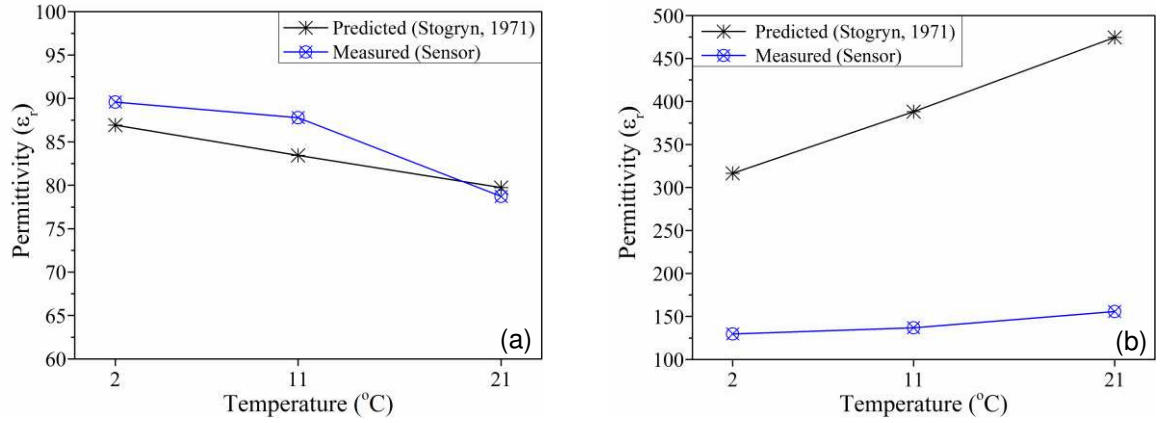

Figure 14: Temperature influence on the sensor output when immersed in **(a)** fresh water and **(b)** saline water of 35 ppt.

In conclusion, the instrument appears to be capable of monitoring the dielectric permittivity in the range ε_r = 1-150 ($\sqrt{\varepsilon_r}$ = 1-12.25) and to provide an accurate measurement in the range ε_r = 1-80.46 ($\sqrt{\varepsilon_r}$ = 1-8.97) regardless of the source of medium (i.e. nature of the liquid, temperature, or salt concentration).

5.2. Calibration of the soil mixing model

The effect of soil water content on the sensor response was validated and found to agree with the calibration curve provided by the manufacturer. However, no information was available regarding the influence of soil density on the sensor output. This study estimates this influence using equations (3) and (4), which then enables discrimination between in-situ and deposited soil conditions.

Figure 15(a) presents the sensor response in four samples having a nominal water content of 10% (10.03 %, 11.20 %, 9.98 % and 10.59 %) and prepared at different density values of 1.06 g/cm^3, 1.30 g/cm^3, 1.41 g/cm^3 and 1.44 g/cm^3 respectively. As shown in figure 15(a), soil density has a noticeable effect on the permittivity output obtained from the sensor. This is associated with the decreased volume of voids of the three phase sample due to increased soil density, and to the larger apparent permittivity of the solids (ε_s = 4-5) when compared to air (ε_a = 1). The experimental data in figure 15(a) then allowed the determination of the optimum parameter α for the soil mixing model using a non-linear least square error regression. Figures 15(a) and 15(b) show the values predicted by equation (1) based on the best fit value of α = 0.478 together with the values determined experimentally.

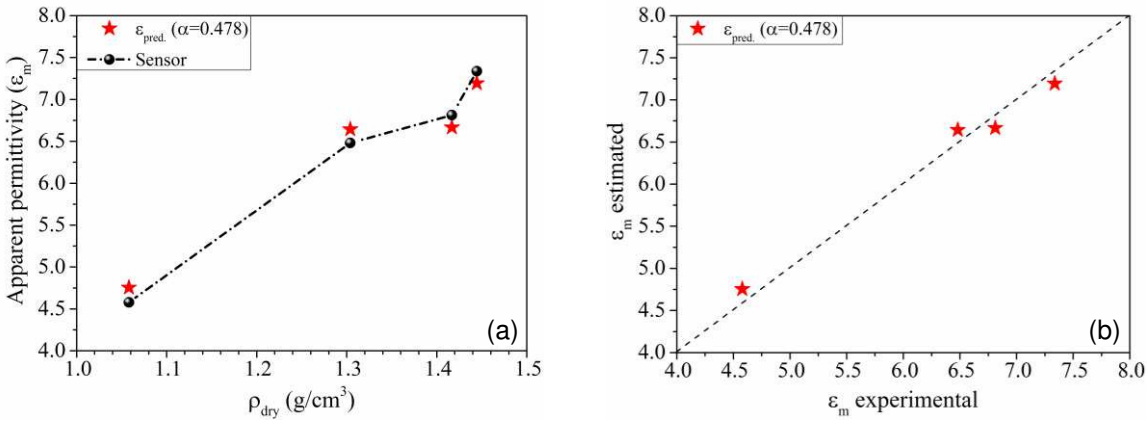

Figure 15: (a) Density effect on the sensor output and **(b)** optimum factor α for estimated and experimental permittivity values obtained with non-linear least square error analysis.

Note that the best-fitting parameter α of 0.478 is consistent with the values reported in the literature which found to be in the range from 0.46 to 0.50 [18, 19, 27, 28]. These

experimental results, allowed calibrating the mixing model and enabling equation (3) to be used to infer soil porosity from dielectric permittivity readings.

5.3. 'Static' scour test results

The sensor response when embedded into gravel, coarse sand and medium sand soil types mixed with fresh water, is shown in figure 16(a). After removal of the sediment (i.e. scour conditions), a sharp increase of the obtained apparent permittivity value occurs due to a change of the surrounding medium at the location of the sensor. Note also that, for gravel soil type, the obtained permittivity when the sensor was embedded into the sediment is greater by approximately 7 when compared to the other tested mediums. This permittivity difference between the tested soil types is likely to be associated with changes in the soil porosity value in the local region around the sensor location, which is influenced by the soil particle shape and orientation in the surrounding area of the two electrodes. From equation (3), the porosity for $\alpha = 0.478$ was then calculated for each tested soil type, as presented in figure 16(b).

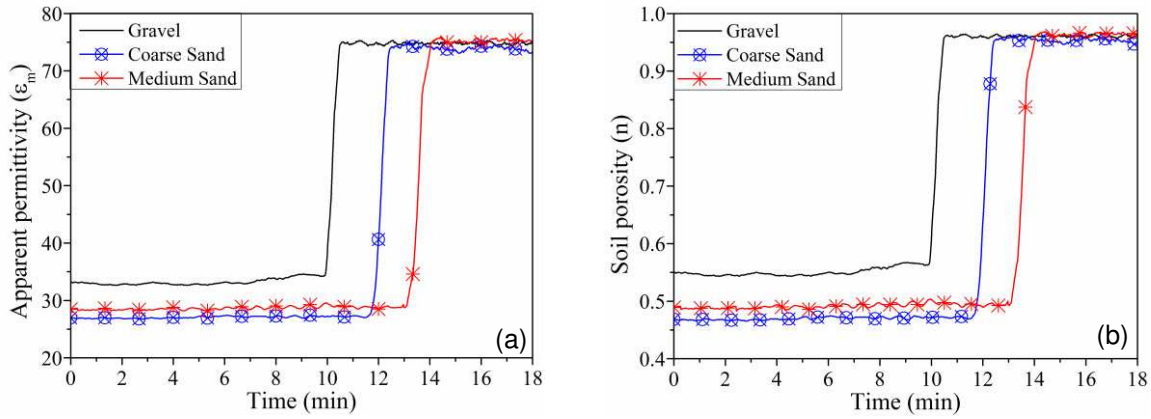

Figure 16: (a) Sensor permittivity outputs and **(b)** estimated soil porosity (n) values obtained for the optimum α factor during 'static' scour tests.

The probe was subsequently tested in saline water of 35 ppt using the aforementioned soil types. The experimental results obtained during these tests using saline water were then compared to the permittivity values predicted using the equation of Debye form as proposed by Stogryn [26]. Assuming that the porosity of each tested medium remains the same between the experiments carried out in fresh and saline water, the only variable in equation (2) is the permittivity of saline water. The permittivity of the saline aqueous solution of 35 ppt at temperature of 11 ^{o}C was calculated from Stogryn [26] as $\varepsilon_{ws} = 388.1$, and then equation (2) was used to infer the overall apparent permittivity. The estimated apparent permittivity value was then compared to the experimentally obtained output for each soil type as presented in Fig. 17. Before scour conditions the sensor output in gravel soil type remained below the estimated

permittivity values, as shown in figure 17(a). A satisfactory agreement is detected between estimated and experimental permittivity values for coarse sand and medium sand soil types, as presented in figures 17(b) and 17(c) respectively. The slight difference between the predicted and measured output in the tests using gravel soil type suggests that re-calibration of the parameter α is required for sediments with dissimilar characteristics compared to sand mediums. In particular, this discrepancy is caused by the overall greater permittivity value that was detectable in gravel sediments when compared to sand mediums. For field deployments, calibration of the parameter α is in principle required for the sediment where the probe is going to be installed. This can be achieved by testing at least one sample of known porosity η and back-calculating α using equation (3). However, it is worth noticing that the value obtained for the material tested in this programme ($\alpha = 0.478$) is very close to the value $\alpha = 0.5$ proposed by Birchak *et al* [19] and Whalley [29] investigating different granular materials. As a result, a value of $\alpha = 0.5$ can be assumed as a first approximation if no specific calibration can be carried out.

After scouring, for all the tested soil types in saline water a large difference between estimated and measured outputs is observed, as shown in figure 17. This phenomenon is mainly attributed to the limitation of the instrument with regard to voltage output range, as was presented in figures 12, 13 and 14.

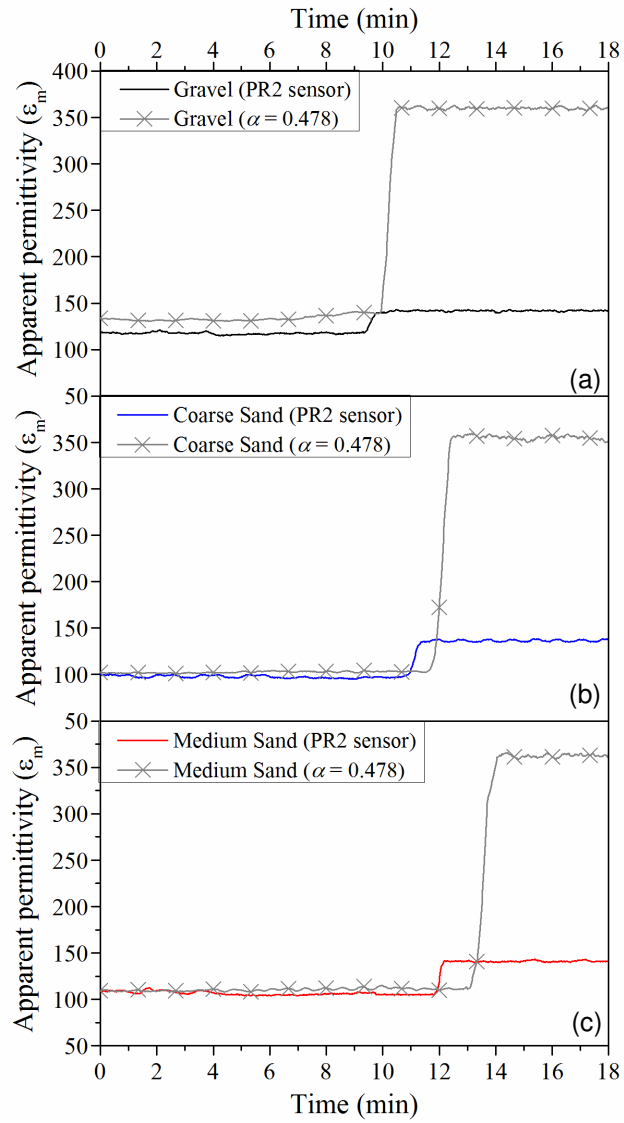

Figure 17: Measured and estimated permittivity values for the sensor embedded in **(a)** gravel **(b)** coarse sand and **(c)** medium sand sediments using saline water of 35 ppt.

Based on the porosity values obtained in fresh water, the dielectric permittivity was satisfactorily estimated in saline water for sand sediments. Despite also the inability of the probe to measure properly the greater permittivity in saline water of 35 ppt of NaCl, a significant change in sensor output is still observed, which would permit monitoring of bed level variations in water with high salinity concentrations. In environments where water salinity is anticipated to fluctuate over time (e.g. river mouths), it might be difficult to discriminate the effects of salinity and density on the permittivity, i.e. a change in salinity may generate a variation in permittivity that could be (mis)interpreted as a change in sediment density. This problem can be overcome by monitoring the signal of a sensor placed above the riverbed and therefore permanently exposed to water conditions. The change in signal of the water-exposed sensor can be then used to infer the change in salinity concentration, which in turn will enable

to correct measurements of the sensors embedded in the original or re-sedimented riverbed. The reading of the water-exposed sensor also allows determining ε_w which can be replaced in equation (3) to calculate the soil porosity. This correction could also be achieved by inspecting the signal of the deepest sensor embedded in the portion of riverbed that was never scoured and therefore never experienced a change in density.

5.4. Real-time flume experiments

5.4.1. Saturation process of the riverbed segment

Figure 18 presents the apparent permittivity values derived from equation (5) during the saturation of the flume riverbed segment that consisted of coarse sand mixture and medium sand soil types each time. Prior to the saturation process, sensors S2, S3 and S4 were embedded into the dry sediment and the corresponding permittivity values ranged from 3 to 4 (see figure 18). When the saturation process is initiated, the permittivity value for sensor S2 increases sharply followed by S3 and S4 responses. Once saturation of the riverbed segment is complete, the permittivity values for the three sensors settle between 23 and 32 for both sediment types. For the duration of the experiment, the permittivity observed by sensor S1 remains constant and equal to 1, as it is located outside the tested section in air environment.

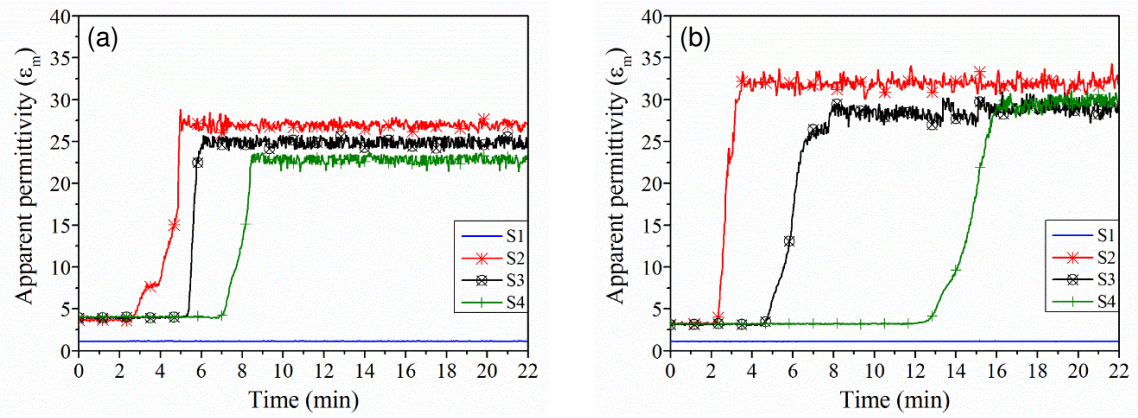

Figure 18: Permittivity values obtained in **(a)** coarse sand and **(b)** medium sand sediments during the saturation process of the riverbed segment.

The saturation tests using the flume indicated that water infiltration of the riverbed segment had a significant increasing effect on the apparent permittivity values obtained by the sensor signals.

5.4.2. Real-time flume tests results

Figure 19(a) shows the scour probe response, the location of the sensors in the tested section and the measured scour depth obtained in coarse sand mixture sediment. Initially, the measured

apparent permittivity of the water-immersed sensor (S1) was at the range of 78. At the same time, the sensors (S2, S3 and S4) that were embedded into the sediment exhibited permittivity values below 27. As figure 19(a) indicates, after a period of 1 hour the scour depth increased to 7.2 cm. At the same period of time, it was observed that the output of S2 increased to 75 and thereafter remained almost constant. This change in the S2 is due to the different permittivity which reveals that the sediment around the sensor location is scoured, i.e. the soil is replaced by water.

During the same time period, the S3 output increased only marginally, which indicates that the scouring on S2 insignificantly influenced the S3 output. The scour depth continued to rise and at the period of 2.5 hours was recorded at 15.7 cm. At the same time the S3 output was increased sharply and reached permittivity in the range of 75. Thereafter, the signals of the scoured S2 and S3 sensors remained steady whereas scour reached its equilibrium at depth of 17.5 cm. The sediment deposition process started after a period of 5 hours and the S3 permittivity output dropped to 37 as the area around the sensor level was re-filled with sediment and scour depth was reduced to 12.7 cm. After 6 hours, the S2 permittivity also declined to 34 while S3 continued to decrease further to 33. As shown in figure 19(a), at the same time measured scour depth was 2 cm indicating that the sediment around both S2 and S3 corresponded to re-deposited saturated sediment. Finally, scour depth did not reach the location of S4 so it exhibited steady permittivity values of 23 throughout the experiment. Figure 19(a) demonstrates that different measured permittivity values were obtained for conditions that corresponded to pre-scour and post-sediment deposition.

Figure 19(b) presents the sensor outputs and scour depth recorded for medium sand soil type. S1 remained submerged in water and exhibited permittivity values at the range of 77. S2 and S3 sensors were embedded into the riverbed segment and their outputs at the beginning of the flume test were recorded around 30 and 29 respectively. Thereafter, a rise of the S2 output was observed reaching values between 68 and 81 while a parallel increase of the scour depth to 7.2 cm occurred.

As shown in figure 19(b), almost 4.5 hours after the experiment was initiated, the S3 permittivity value increased from 30 to 49. For the same time period, scouring also increased and reached its maximum depth of 12.9 cm. Then, after 6 hours, scour depth decreased to 8 cm while the value of S3 also reduced to 32. The slight variation of the S3 output reveals that scour depth reached but did not fully expose this sensor in water conditions. The decrease of the measured scour depth and S3 values that occurred after the maximum recorded scour depth corresponds to the physical process of sediment transportation in the flume and deposition in

the riverbed segment around the location of S3. An equivalent decrease in both the measured scour depth and the signals of S2 and S3 was observed when the simulation of sediment deposition was initiated after the period of 6 hours [see figure 19(b)]. Finally, the recorded permittivity output of S2 and S3 after the sediment deposition simulation reached values similar to as pre-scour conditions (31 mV and 29 mV respectively) while scour depth decreased to 1.5 cm. During this test the permittivity output of S4 was almost constant at the range of 29, which indicates that it was not affected by scour and remained embedded in the sediment. It is also pointed out that when the sensors are fully exposed to water conditions, the permittivity readings have considerable variance over time. This is attributed to water turbulence and variability of solids that are suspended in water near the sensor vicinity. This large captivation of the sensor signal over time can therefore be employed as a secondary validation that the sensor is fully scoured and exposed to water conditions.

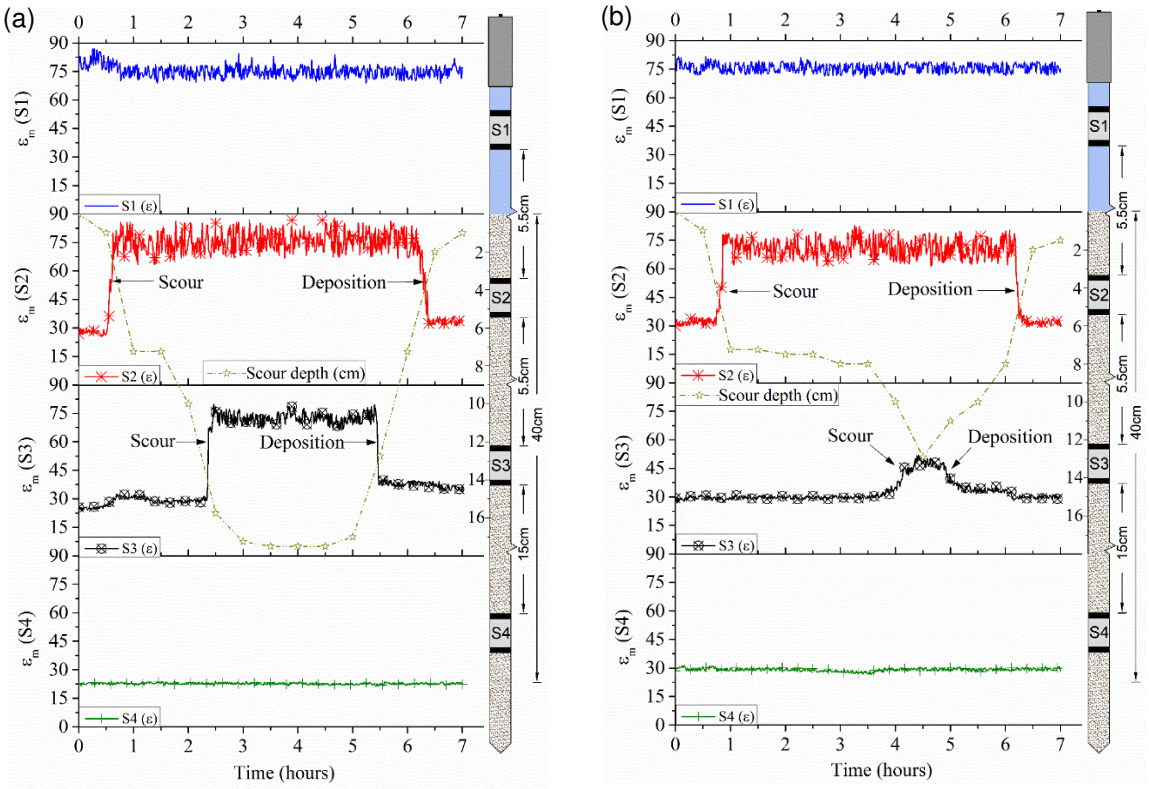

Figure 19: Measured permittivity values and scour depth during flume experiments in **(a)** coarse sand mixture and **(b)** medium sand sediments. The measured scour depth and the location of each sensor along the probe length are also presented for each flume test.

The dry density for $\alpha = 0.478$ was then estimated from equations (3) and (4) in order to obtain the soil density at the location of each sensor for both experiments. Figure 20(a) shows the predicted soil density obtained in coarse sand mixture sediment, which at the start of the experiment varied between 1.5 gr/cm^3 (S2), 1.6 gr/cm^3 (S3) and 1.7 gr/cm^3 (S4). After sediment re-deposition, the density values for S2, S3 were recorded at the range of 1.2 gr/cm^3 and 1.3

gr/cm^3 respectively, while the S4 was not affected by scour processes during the experiment. Figure 20(a) demonstrates that different soil density conditions occurred when the sensor was embedded to in-situ soil compared to re-deposited sediment.

As figure 20(b) shows, for medium sand sediment type the obtained soil density based on the output of sensors S2 and S3 exhibited similar levels for pre-scour and post-sediment deposition conditions of 1.3 gr/cm^3 to 1.4 gr/cm^3 respectively. The water-immersed (S1) and the permanently soil-embedded (S4) sensors were unaffected by the aforementioned processes during the experiment and exhibited density values at the range of 0.0 gr/cm^3 and 1.4 gr/cm^3 respectively [see figure 20(b)].

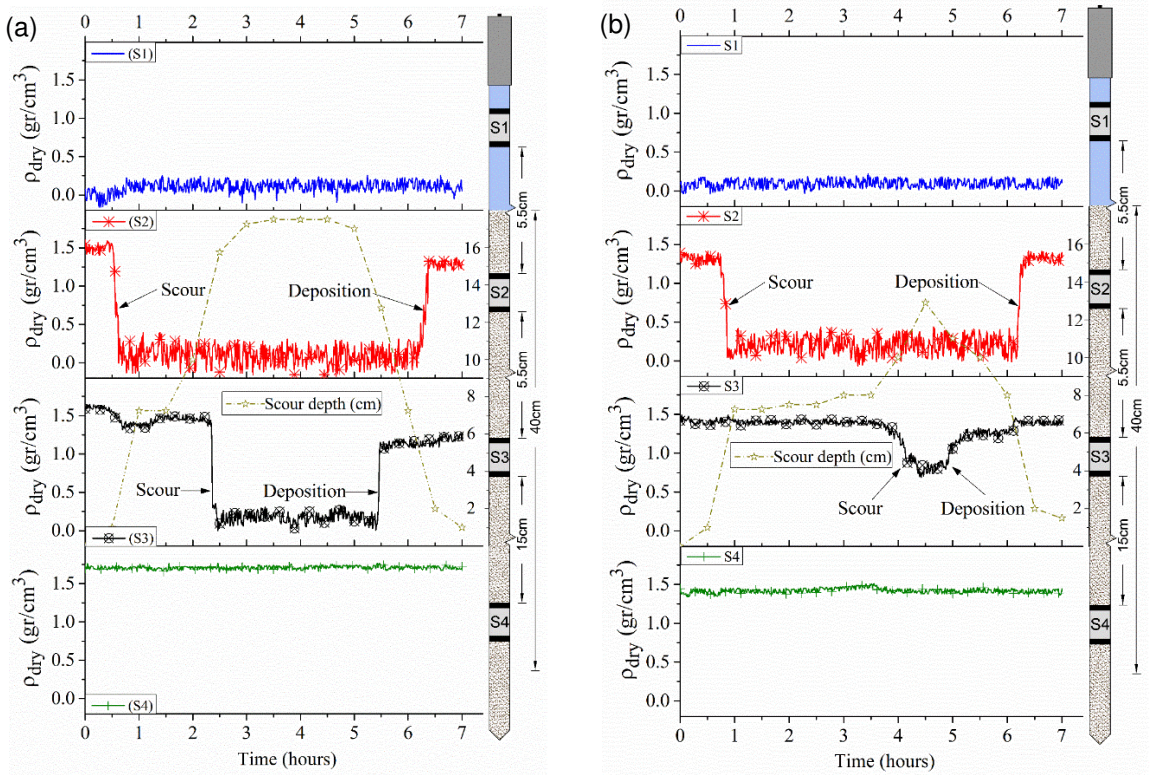

Figure 20: Estimated density values and scour depth during flume experiments in **(a)** coarse sand mixture and **(b)** medium sand sediments. The measured scour depth and the location of each sensor along the probe length are also presented for each flume test.

The results obtained in separate open channel flume experiments using coarse and medium sand sediments clearly demonstrate that the sensors accurately tracked the evolution of both scour and sediment deposition. A sharp increase of the sensors' permittivity output was recorded when scour occurred at the sensor location. Re-deposited sediment was found to be associated with higher apparent permittivity, reflecting the lower soil density around the local regions of each sensor. The sensor is therefore potentially capable of detecting re-deposited sediments characterised by lower density than the original in-situ soil.

6. Conclusions

Scour action is a challenge for civil infrastructure systems due to the changing climate bringing more active weather systems. Bed level conditions at underwater foundations are very difficult to evaluate, considering that scour holes are often re-filled by deposited loose material that is easily eroded during subsequent smaller-scale flood events. The lack of instrumentation techniques available to assess underwater conditions at the foundation structure has in the past led to the sudden collapse of several bridges without prior warning.

This study has presented a new monitoring technique that can be deployed and allows the continuous monitoring of scour depth variations and sediment re-deposition processes at foundation elements. The sensing principle employs the Amplitude Domain Reflectometry (ADR) technique that utilises the reflection characteristics of electromagnetic waves and was evaluated using an off-the-shelf small-scale probe. The ADR instrument was connected to a wireless interface that could allow the real-time remote monitoring of the obtained data.

A systematic series of experimental tests was carried out evaluating the calibration of the instrument and its sensitivity to salinity and temperature effects. A large discrepancy observed between predicted and measured sensor output in saline water was attributed to the limit capability of the instrument's dynamic range. The calibration curve provided by the manufacturer was found to be accurate for apparent permittivity values up to 80. Based on the obtained results three areas were identified on the sensor's calibration curve indicating the accurate (i), the uncertain accuracy (ii) and the out of range (iii) regions.

The use of the sensor signals to discriminate between in-situ and re-deposited soil was also addressed in this investigation. Experimental data obtained at various soil density conditions were employed to calibrate a three phase mixing model with the determination of the optimum geometric parameter α, which was found to be consistent with values reported in the literature. The overall apparent permittivity value was then adequately estimated for sediments with similar characteristics. It was then demonstrated that the soil porosity around each sensor location could also be estimated based on the sensor outputs for sediments with similar characteristics.

This study also thoroughly validated the ADR sensor platform in real-time flume experiments which exhibited high sensitivity to scour and sedimentation processes. Re-deposited sediment was found to be associated with higher permittivity attributed to lower soil density that was successfully estimated. Analysis of the sensor signals demonstrated the ability

of the proposed system to differentiate between pre-scour and post-sediment deposition conditions.

The proposed sensing technique can provide a more economical, accurate and real-time alternative to existing scour inspection methods. The results presented in this investigation provide an important guide and can be used as a benchmark for the field application of the ADR sensor which can be integrated into a structural health monitoring system, delivering key information regarding bed level conditions at foundation elements.

Acknowledgments: The authors would like to thank the reviewers for their constructive feedback and Dr M. Saafi for the assistance in the introductory part of the article.

References

[1] Wardhana K and Hadipriono F 2003 Analysis of Recent Bridge Failures in the United States J. Perform. Constr. Facil. 17(3) 144–150

[2] Richardson E V and Davis S R 2001 Evaluating scour at bridges FHWA NHI 01-001: Hydr. Engrg. Circular No. 18 4th Ed. US Department of Transportation Washington DC

[3] Rail Safety and Standards Board 2004 Impact of scour and flood risk on railway structures Rail Safety & Standards Board Infrastructure Integrity Research Project Number T112 London UK

[4] Rail Safety and Standards Board 2005 Safe Management of Railway Structures Flooding & Scour Risk Rail Safety & Standards Board Research Programme Engineering London UK

[5] Jongman B, Hochrainer-Stigler S, Feyen L, Aerts J C J H, Mechler R, Botzen W J W, Bouwer L M, Pflug G, Rojas R and Ward P J 2014 Increasing stress on disaster risk finance due to large floods Nature Climate Change 4 264–268

[6] Hunt B E 2009 Monitoring scour critical bridges NCHRP synthesis 396 Transportation Research Board Washington DC

[7] Arjwech R, Everett M E, Briaud J-L, Hurlebaus S, Medina-Cetina Z, Tucker S and Yousefpour N 2013 Electrical resistivity imaging of unknown bridge foundations Near Surface Geophysics 11(6) 591-598

[8] Gorin S R and Haeni F P 1989 Use of surface-geophysical methods to assess riverbed scour at bridge piers US Geological Survey Water-Resources Investigations Rep. No. 88-4212 Federal Highway Administration Hartford CT

[9] Placzek G and Haeni F P 1995 Surface-geophysical techniques used to detect existing and infilled scour holes near bridge piers Water Resources Investigations Report 95-4009 US Geological Survey Storrs CT

[10] Forde M C, McCann D M, Clark M R, Broughton K J, Fenning P J and Brown A 1999 Radar measurement of bridge scour NDT & E Int. 32(8) 481–492

[11] Mueller D S and Landers N M 1999 Portable Instrumentation for Real-time Measurement of Scour at Bridges Federal Highway Administration Report FHWA-RD-99-085 McLean VA

[12] Schall J D and Price G R 2004 Portable Scour Monitoring Equipment NCHRP Report 515 Transportation Research Board Washington DC

[13] Yankielun N and Zabilansky L 1999 Laboratory Investigation of Time-Domain Reflectometry System for Monitoring Bridge Scour J. Hydraul. Eng. 125(12) 1279–1284

[14] Yu X and Yu X 2009 Time Domain Reflectometry Automatic Bridge Scour Measurement System: Principles and Potentials Structural Health Monitoring 8(6) 463-476

[15] Lin Y B, Lai J S, Chang K C and Li L S 2006 Flood scour monitoring system using fiber Bragg grating sensors Smart Mater. Struct. 15(6) 1950–1959

[16] Zarafshan A, Iranmanesh A and Ansari F 2012 Vibration-Based Method and Sensor for Monitoring of Bridge Scour J. Bridge Eng.17(6) 829–838

[17] Whalley W R, Dean T J and Izzard P 1992 Evaluation of the Capacitance Technique as a Method for Dynamically Measuring Soil Water Content J. Agric. Engng. Res. 52 147-155

[18] Roth K R, Schulin R, Fluhler H and Attinger W 1990 Calibration of Time Domain Reflectometry for Water Content Measurement using a Composite Dielectric Approach Water Res. Res. 26(10) 2267-2273

[19] Birchak J R, Gardner C G, Hipp J E and Victor J M 1974 High dielectric constant microwave probes for sensing soil moisture Proc. IEEE 62(1) 93–98

[20] Dobson M C, Ulaby F T, Hallikainen M T and El-Rayes M A 1985 Microwave dielectric behavior of wet soil part II: Dielectric mixing models IEEE Trans. Geoscience and Remote Sensing GE-23(1) 35-46

[21] Delta-T Devices Ltd 2006 Moisture content sensor and related methods International Patent Publication WO 2006/064266 A1

[22] Delta-T Devices Ltd 2008 User Manual for the Profile Probe: type PR2 Cambridge UK

[23] Maryott A A and Smith E R 1951 Table of dielectric constants of pure liquids Circular 514 Washington US

[24] Michalis P, Saafi M and Judd D M 2013 Capacitive Sensors for Offshore Scour Monitoring Proc. of the ICE – Energy 166(4) 189–196

[25] Michalis P, Saafi M and Judd D M 2012 Integrated Wireless Sensing Technology for Surveillance and Monitoring of Bridge Scour Proceedings of the 6th Int. Conference on Scour and Erosion Paris France 27- 31 August 2012 395-402

[26] Stogryn A 1971 Eqs. for Calculating the Dielectric Constant of Saline Water IEEE Trans. On Microwave Theory and Techniques 19(8) 733-736

[27] Weitz A M, Grauel W T, Keller M and Veldkamp E 1997 Calibration of TDR technique using undisturbed soil samples from humid tropical soils of volcanic origin Water Res. Res. 33(6) 1241-1249

[28] Yu C, Warrick A W, Conklin M H, Young M H and Zreda M 1997 Two- and three-parameter calibrations of time domain reflectometry for soil moisture measurement Water Res. Res. 33 2417-2421

[29] Whalley W R 1993 Considerations on the use of time domain reflectometry (TDR) for measuring soil water content J. Soil Sci. 44 (1) 1–9